Effects of Brownian force and pore structure on the removal of nanoparticles by porous membranes

Chemical Engineering Science 316 (2025) 122010

Contents lists available at ScienceDirect

Chemical Engineering Science

journal homepage: www.elsevier.com/locate/ces

Effects of Brownian force and pore structure on the removal of nanoparticles by porous membranes

Takashi Hashimoto [a,*], Alberto Tiraferri [b], Satoshi Takizawa [a,c]

[a] Research Center for Water Environment Technology, Graduate School of Engineering, the University of Tokyo, 7-3-1 Hongo, Bunkyo-Ku, Tokyo 113-8656, Japan
[b] Department of Environment, Land and Infrastructure Engineering (DIATI), Politecnico di Torino, Corso Duca degli Abruzzi, 24 10129 Torino, Italy
[c] Department of Urban Engineering, Graduate School of Engineering, the University of Tokyo, 7-3-1 Hongo, Bunkyo-Ku, Tokyo 113-8656, Japan

ARTICLE INFO

Keywords:
Brownian force
Membrane filtration
Particle transport
Péclet number
Virus removal

ABSTRACT

This study investigated the effects of Brownian force on the transport and retention of nanoparticles within the pores of water filtration membranes using COMSOL Multiphysics®. Simulation results suggest that, at Péclet numbers below 10, the Brownian force may increase the frequency of nanoparticle collisions with pore walls to substantially increase log reduction rates (LRVs). Indeed, the LRVs increased linearly with attachment coefficient values; even at a low attachment coefficient of 0.001, high LRVs over 1.5 were observed under some geometries owing to the high frequency of nanoparticle-wall collisions. The calculated LRVs were inversely correlated with the Péclet numbers, whereas the slope of the inverse correlation was dependent on the membrane pore size. Complex structures, such as pore constriction, tortuosity, and non-uniform pore size, increased the LRV, whereas the overall porosity was not a determinant removal factor within the pores. In the configuration with parallel large and small pores, the Brownian force increased the number of nanoparticles entering the membrane through small pores relative to the numbers estimated based on water flow rates. These results indicate that the Brownian force may be an important particle removal factor within membrane pores under certain conditions; this should be considered when designing and operating membrane filters.

1. Introduction

The emergence of de facto and direct potable water reuse of municipal wastewater requires high removal rates of nanoparticles and pathogenic microorganisms, including viruses, to ensure drinking water safety (Gerba et al., 2017; Sano et al., 2016). Although low-pressure porous membrane processes such as microfiltration (MF) and ultrafiltration (UF) are commonly used as pretreatments for reverse osmosis (RO) membrane filtration, the virus log reduction rates (LRVs) they provide vary extensively (ElHadidy et al., 2013; Huang et al., 2012). Previous studies have reported that the main factors influencing virus removal rates are membrane nominal pore sizes (Huang et al., 2012; Yin et al., 2015), pore size distribution (Giglia et al., 2015), water quality and matrix composition (Lee et al., 2017), and the interaction between viruses and membrane materials (Chaudhry et al., 2015; Yasui et al., 2024). While these studies revealed the influence of individual aggregate parameters on virus removal by porous membranes, studies on the influence of the driving forces of particle motion within membrane pores on virus removal rates are limited despite the significant influence of membrane microstructure on the removal rates of viruses (Calo et al., 2015).

The hindered transport theory was proposed to describe particle transport within cylindrical membrane pores as a function of convection and diffusion terms, including steric and hydrodynamic hindrance factors (Brenner and Gaydos, 1977; Deen, 1987). However, because the effects of these factors are typically averaged over the entire cross-section of a pore, this theory only applies to cylindrical pores (Dechadilok and Deen, 2006). Moreover, studies on virus transport through membrane filters based on hindered transport theory have largely neglected the diffusion term, assuming low pore-to-particle size ratios and high filtration velocities (ElHadidy et al., 2013; Zeman and Zydney, 1996). Consequently, the hindered transport theory cannot be applied to estimate virus and nanoparticle removal by membranes characterized by small and complex pore structures or at low ratios of convection against Brownian transport of particles, which is expressed as the Péclet number.

The transport of colloidal particles through porous media has been described by depth filtration models incorporating particle advection,

* Corresponding author.
E-mail addresses: hashimoto@env.t.u-tokyo.ac.jp (T. Hashimoto), alberto.tiraferri@polito.it (A. Tiraferri), takizawa@env.t.u-tokyo.ac.jp (S. Takizawa).

https://doi.org/10.1016/j.ces.2025.122010
Received 6 April 2025; Received in revised form 7 June 2025; Accepted 8 June 2025
Available online 9 June 2025

hydrodynamic diffusion, and deposition, typically employing a one-dimensional advection–diffusion partial differential equation (Tufenkji and Elimelech, 2004). Colloid filtration theory (CFT) is most commonly used to describe the deposition rates of colloidal particles in porous media as the sum of contributions from three individual retention mechanisms: Brownian diffusion, interception, and sedimentation (Yao et al., 1971). The deposition rate of colloids onto porous media by diffusion and interception are governed by the total interaction energy between colloids and media surfaces (Tufenkji and Elimelech, 2004). The CFT has been successfully applied to describe the transport of particles greater than 1 μm in granular filtration and soil media, which have larger pores than membrane filters, in many cases by more than ten-fold (Boccardo et al., 2019; Yao et al., 1971). In addition, CFT considers the filter bed as an assemblage of unit collectors and is based on the concept of single-collector removal efficiency, which is hardly applicable to the typical morphology of filtration membranes (Nelson and Ginn, 2011). Membrane filters are commonly used to remove particles smaller than those targeted by granular filters (Molnar et al., 2016; Tufenkji and Elimelech, 2005a). These smaller particles with higher diffusivity may deposit onto pore surfaces even under unfavorable interaction conditions, when the Brownian kinetic energy exceeds the repulsion energy barrier between particles and surfaces (Hashimoto-Gotoh et al., 2015).

Owing to Brownian forces, small pore sizes, and complex pore structures, it remains difficult to predict the removal rates of nanoparticles, including viruses, using membrane filtration processes (Giglia et al., 2015; Hashimoto-Gotoh et al., 2015). Although the complex microstructures of porous membranes influence liquid flow and particle transport (Mondal et al., 2019), previous studies on particle transport in a complex microstructure were conducted based on Darcy's law at the macroscopic scale because of the limitations of experimental techniques at the microscale (Bowen and Welfoot, 2002; Iliev et al., 2017). Therefore, computational simulations of membrane filtration processes are often used to investigate particle transport within membrane pores at a fraction of the experimental cost (Dalwadi et al., 2015). Computational simulations have been employed to elucidate the influence of the membrane morphology, including porosity (Sanaei and Cummings, 2017), pore interconnectivity (Gu et al., 2020), and tortuosity (Griffiths et al., 2020). These studies simulated the influence of membrane pore microstructures on the flow dynamics and colloidal particle motion. However, the Brownian force was not integrated into these simulation models, although it may influence the colloidal particle motion (Hashimoto-Gotoh et al., 2015). Other studies on particle transport in membrane pores have employed simulation models built and run under limited conditions without integrating the Brownian forces (Mino et al., 2018; Mondal et al., 2019). Recent experimental and simulation studies on virus or nanoparticle removal via membrane filtration have proposed the diffusional deposition of nanoparticles onto the pore wall (Lee et al., 2020) or remobilization of viruses captured by size exclusion mechanisms (Gustafsson et al., 2018) as the effects of Brownian force. However, the detailed mechanisms behind these proposed effects associated with Brownian force have not yet been addressed.

Recent advances in three-dimensional (3D) visualization and reconstruction techniques have enabled the simulation of liquid flow and particle transport in porous membrane microstructures (Ley et al., 2018; Sundaramoorthi et al., 2016). However, these approaches have the limitations of high computational cost in simulating the entire membrane structure and are associated with frequent errors in creating 3D models (Tan et al., 2023). Moreover, although 3D simulations can reconstruct the complex microstructures of porous membranes, simulations of the actual membrane behavior make it difficult to compare and isolate the various factors influencing the transport and retention of nanoparticles within membrane pores. Thus, simplified models representing different parameters and characteristics of membrane pores would be useful in highlighting the effects of individual and combined parameters.

Therefore, this study aims to evaluate the effects of Brownian force relative to drag force and structural characteristics of membrane pores on the transport and retention of nanoparticles within membrane pores, using two-dimensional simulation models built in COMSOL Multiphysics®. The simulation models incorporated drag and Brownian forces to evaluate their influence. The effects of pore diameter, length, tortuosity, and shape on particle retention are discussed based on the simulation results obtained under a wide range of Péclet numbers. The comprehensive set of geometries and simulation conditions allow the assessment of the relative importance of the Brownian force in particle retention inside a membrane and the identification of the membrane features that would augment or reduce retention by this mechanism.

2. Materials and methods

2.1. Numerical simulation

Particle transport within membrane pores was simulated using COMSOL Multiphysics® v 6.1 with the Particle Tracing Module. COMSOL Multiphysics® applies the finite-element-method to simulations of fluid flow by solving Navier-Stokes equations (Eq. (1)). The particle-tracing module simulates the trajectory of the particles using the Lagrangian approach by solving ordinary differential equations using Newton's law of motion (Eq. (2)). The Stokes drag and Brownian forces were incorporated independently or combined into the simulation models as forces acting on particles within the membrane pores. The Navier-Stokes equations are as follows:

Momentum equation: $\rho\nabla u = -\nabla p + \mu\nabla^2 u$

Continuum equation:

$$\nabla\cdot u = 0 \tag{1}$$

where ρ is the density of the fluid [kgm^{-3}], u is the velocity vector [ms^{-1}], p is the pressure [$kg\ m^{-1}s^{-2}$], and μ is the fluid dynamic viscosity [$kg\ m^{-1}s^{-1}$].

The Newton's equation of motion implemented in the simulations is as follows:

$$m_p\frac{dv_p}{dt} = F_D' + F_B \tag{2}$$

where m_p is the particle mass, v_p is the particle velocity vector, and F_D' and F_B are the drag force with wall corrections based on the Stokes drag law and Brownian force, respectively, as defined by Eqs. (3) and (4)):

$$F_D' = \frac{18\mu}{\rho_p {d_p}^2} m_p M(u - v_p) \tag{3}$$

where ρ_p is the particle density, d_p is the particle diameter [m], M is the wall correction factor defined by Eq. S1 in Appendix.

$$F_B = \zeta\sqrt{\frac{12\pi\lambda d_p \mu k_B T}{\Delta t}} \tag{4}$$

$$\lambda = \left(1 - \frac{d_p}{d_{pore}}\right)^3$$

where k_B is the Boltzmann constant, T is the absolute temperature [K], Δt is the magnitude of the time step [s], d_{pore} is the pore diameter [m], λ is a correction factor of particle-to-pore diameter, ζ is a normally distributed random number with a mean of zero and unit standard deviation. The random direction of the Brownian force was accounted for by evaluating both the x and y components of F_B at each time step using independent values of ζ in the two directions. In this simulation, the relative tolerance, which determines the simulation time step Δt, was carefully selected to ensure that the influence of Δt on the particle behavior in the Brownian force simulation was negligible.

2.2. Simulation of water flow and particle transport in membrane pores

This study simulated the water flow and particle transport in two-dimensional pore model geometries as described in **2.3**. All the simulation models assumed laminar flow with no-slip boundary conditions on the pore wall. Time stepping for the numerical integration of the Langevin equation was set at 10^{-4} s, which was two orders of magnitude smaller than the simulation time of 10^{-2} s and sufficiently small to achieve the convergence of simulation results. At least triplicate simulations were run for each condition to examine convergence of LRV values.

Unless otherwise specified, the *trans*-membrane pressure was set at 20 kPa between the feed and filtrate sides of membrane pores, with a pore length of 175 μm, chosen based on the typical thickness of a microfiltration PVDF membrane (Fig. S1). Assuming the properties of small viruses, spherical particles with a diameter of 0.02 μm and a density of 1,020 [kg/m^3] were released at the pore inlet at $t = 0$ with the initial velocity and distribution based on the flow velocity field. A drag force based on the Stokes drag law (Eq. (3)) and/or Brownian force (Eq. (4)) was imposed on the particles traveling through the pores. The Péclet number specifies the relative importance of convection over diffusion, and is defined in Eq. (5):

$$Pe = \frac{6\pi\eta_0\dot{\gamma}r_p^{\,3}}{k_B T} = \frac{r_p^{\,2}\dot{\gamma}}{D} \tag{5}$$

where η_0 is the viscosity of the fluid, $\dot{\gamma}$ is a reciprocal of the shear rate, r_p is the radius of a particle, and D is a diffusion coefficient defined by Eq. S2.

In the simulations, the density of the particles was assumed to be approximately equal to that of water. This property and the results of preliminary simulations, imply the gravitational force acting on the particles was negligible compared to the drag force and was consequently omitted from the simulation. The Particle Tracing module assumes particles as point masses, which is acceptable when the volume fraction of particles is less than 1 % (0.076 % or less in this study). A collision with pore walls occurs when the center of a particle reaches wall geometries. Upon collision, a particle may either attach to the wall following the probability given by the attachment coefficient; otherwise, it is reflected from the wall with incident and reflected angles equal to the surface normal (Eq. S3).

2.3. Pore structures and geometries

Simulation models were built with different membrane pore structures representing and simplifying the complexity of actual membranes, including straight pores with different diameters and lengths, constricted pores with non-uniform pore diameters, and tortuous pores. These models were built to evaluate the effects of Brownian forces and pore structures on particle transport and retention within the pores (Table 1). A finite-element unstructured triangular mesh consisting of 45 000 to 550 000 elements was employed, tailored to the size and shape of

Table 1
Pore structures and geometries investigated in simulations.

Type	Pore geometry	Parameters
1. Straight pores	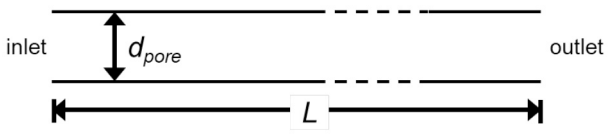	L = pore length d_{pore} = pore diameter
2. Gates in pores	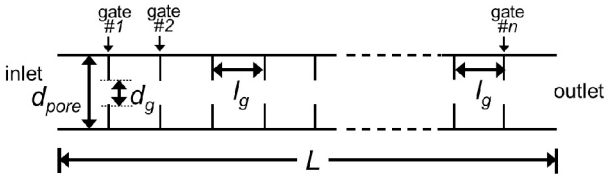	d_g = gate diameter l_g = distance between gates d_g/d_{pore} = diameter ratio
3. Non-uniform pore diameter	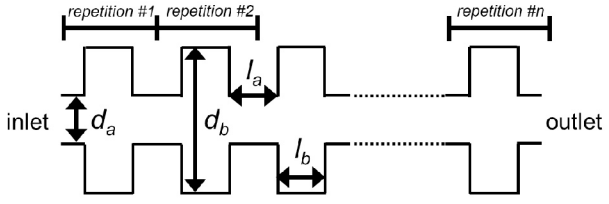	d_a = fixed pore diameter d_b = variable pore diameter l_b/l_a = pore length ratio
4. Pore tortuosity	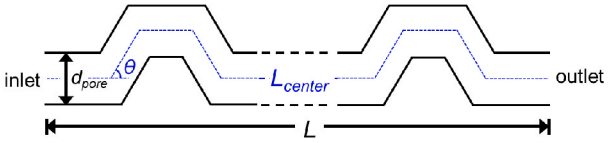	θ = bending angle L_{center} = centerline path length
5. Parallel pores of different diameters	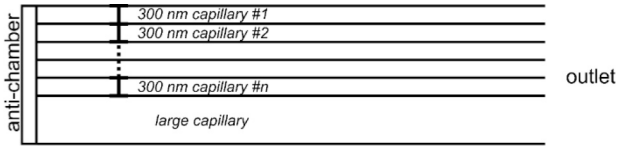	

pore geometries. Finer and coarser mesh settings were explored to identify the optimal mesh conditions for each pore geometry that would lead to the convergence of simulation results within shorter computational times.

2.3.1. Straight pores

The pore length was 175 μm, while the pore diameters varied in the 0.2–1.6 μm (Table 1, Pore geometry 1). For the simulation models with pore diameters of 0.4 and 0.8 μm, the pore length was varied from 17.5 to 175 μm. To fix the average velocity within the pore regardless of the pore length, the pressure difference between the inlet and the outlet of the pores shorter than 175 μm was set to 20 kPa multiplied by the pore length in μm divided by 175 μm.

2.3.2. Gates in pores

To investigate the influence of pore constriction on particle transport at fixed porosity, gates were installed in straight pores with a pore length of 25 μm (Table 1, Pore geometry 2). The *trans*-membrane pressure was set at 2.87 kPa to obtain the same average velocity relative to a *trans*-membrane pressure of 20 kPa in a pore with a length of 175 μm. The gate openings were set to one-third of the pore diameter, whereas the number of gates in the pores varied from 1 to 16. As the thickness of the gate was set to the negligible value of 0.0025 μm, the pore porosity with and without gates was almost equivalent.

2.3.3. Non-uniform pore diameters

Pore models with non-uniform pore diameters were built to simplify the effects of complex pore geometries on water flow and particle retention (Table 1, Pore geometry 3). The pore models were built by combining a diameter equal to 0.3 or 0.6 μm (d_a) and portions of variable pore diameters in the 0.15–4.8 μm (d_b) range. Unless otherwise stated, the non-uniform pore diameters were repeated 10 times in a total pore length of 25 μm. The simulations were conducted at a *trans*-membrane pressure of 2.87 kPa.

2.3.4. Pore tortuosity

Porous membranes exhibit complex structures that are not straight but tortuous (Ghanbarian et al., 2013). This study utilized tortuosity, τ, defined as an elongation factor of the average flow path in a pore (Ghanbarian et al., 2013; Matyka et al., 2008):

$$\tau = \frac{L_{center}}{L} \tag{6}$$

where L_{center} is the centerline path length of a pore and L is the straight distance between the inlet and outlet of a pore, which can be assumed to be the membrane thickness.

The tortuosity of pores is often overlooked in many idealized experimental systems and simulation models such as cylindrical pores (Griffiths et al., 2020). However, tortuosity is a key factor influencing porous membranes' permeability and particle retention (Graczyk and Matyka, 2020). A typical hypothesis is that the high tortuosity of membrane pores increases the likelihood of particle entrapment, mainly because of the extended path length (Griffiths et al., 2020). However, tortuosity changes a pore's path length and flow direction. Therefore, to evaluate the effects of changes in the flow direction, for each geometry, the bending angle between two connecting straight pores was set to a value between 0° (straight pore) and 90° (maximum tortuosity); see Table 1, Pore geometry 4. The centerline path length was 25 μm regardless of the bending angle, and the *trans*-membrane pressure was fixed at 2.87 kPa.

2.3.5. Parallel pores of different diameters

Porous membranes contain unevenly distributed pores of diverse sizes and shapes (Mondal et al., 2019). The effect of pore size distribution on the entrance statistics of nanoparticles at the membrane-feed interface and their subsequent retention within the pores was investigated in this study using geometries consisting of multiple pores characterized by different diameters with varying ratios (Table 1, Pore geometry 5). In these simulations, particles were not released at the inlet of the pores but in a narrow anti-chamber external to the membrane, thus allowing the model to drive particle trajectories into the pores. The particle retention rates obtained from simulations with such geometries were compared with the respective nominal retention rates, $R_{nominal}$, calculated based on the same geometry but by deploying the retention rates determined for individual pores constituting the geometry (Eq. (7)):

$$R_{nominal} = \frac{(q_1 \times n_1 \times R_1) + (q_2 \times n_2 \times R_2)}{(n_1 \times q_1 + n_2 \times q_2)} \tag{7}$$

where n_1 and n_2 are the numbers of small pores of diameter 1 and large pores of diameter 2 in parallel, R_1 and R_2 are the retention rates associated with single pores with diameters of 1 and 2, respectively, and q_1 and q_2 are the respective flow rates. The flow rate was calculated as follows:

$$q = A \times v \tag{8}$$

where v is the average velocity in the pore computed by COMSOL Multiphysics® v 6.1 and A is the cross-section area of the pore (cylindrical structure assumption).

2.4. Attachment coefficient

The retention rates are influenced by interactions between colloidal particles and internal pore surfaces (Trzaskus et al., 2015; Tufenkji and Elimelech, 2004), as well as by hydrodynamic force (Lee et al., 2020). Electrostatic, van der Waals and hydrophobic interactions between two surfaces are featured in classical DLVO (Jacob N. Israelachvili, 2011) and extended DLVO approaches (Brant and Childress, 2002). This study combined the overall interaction forces and the hydrodynamic force into an attachment coefficient, the probability of particle retention on the pore surfaces upon collision. The impact of the attachment coefficient on the retention rate of particles in the membrane pores was preliminarily examined through specific simulations using straight pore models with a diameter of 0.6 μm. Subsequently, its value varied from 10^{-3} to 10^{-1} in the simulations, representing relatively unfavorable and favorable attachment conditions. The value of the attachment coefficient was selected specifically for each geometry to obtain a range of LRVs that confidently highlighted the relative effects of the investigated parameters.

2.5. Particle retention

The retention rates of the particles in the simulation models are presented as log reduction values (LRV) (Eq. (9)):

$$\mathrm{LRV} = -\log_{10}\left(\frac{N_{out}}{N_{in}}\right) = -\log_{10}\left(\frac{N_{in} - N_{att}}{N_{in}}\right) \tag{9}$$

where N_{in} is the number of particles released into the pores at the beginning of the simulation, N_{out} is the number of particles passing through the outlet of a pore, and N_{att} the number of particles attached to the deposited walls is retained within the pore. All simulations were conducted for at least twice the hydraulic retention time (HRT) of each pore structure to allow > 99.8 % of the particles to deposit to pore walls or reach the filtrate end of the membrane. Therefore, $\left(\frac{N_{out}+N_{att}}{N_{in}}\right) > 0.998$ at the end of all the simulations.

3. Results

3.1. Effect of Brownian force

The LRVs of the preliminary pore-flow simulations were compared with and without the Brownian force using straight pore models with different pore diameters (Fig. 1a). Under the investigated conditions, the LRVs of the simulations with Brownian force were significantly higher than the LRVs without Brownian force; namely, they were approximately equal to 1.6 in a pore with a diameter of 1.6 μm and > 3.0 with a pore diameter of 0.4 μm, compared to the LRVs of approximately 0 in the absence of Brownian force. Note that the nominal upper limit of the LRV was 3 logs in these and other simulations discussed below because the number of particles released at the inlet was set at 1000 for each individual simulation. Particle traces showed that the Brownian force caused the random motion of particles, departure from streamlines parallel to the flow directions, and collision against pore walls. In laminar flow at a constant transmembrane pressure, known as Hagen-Poiseuille flow, the flow rate decreases with pore diameter; therefore, the Brownian force may become considerable over the drag force in small pores, as shown by the same LRV results plotted as a function of the Péclet number in Fig. 1b.

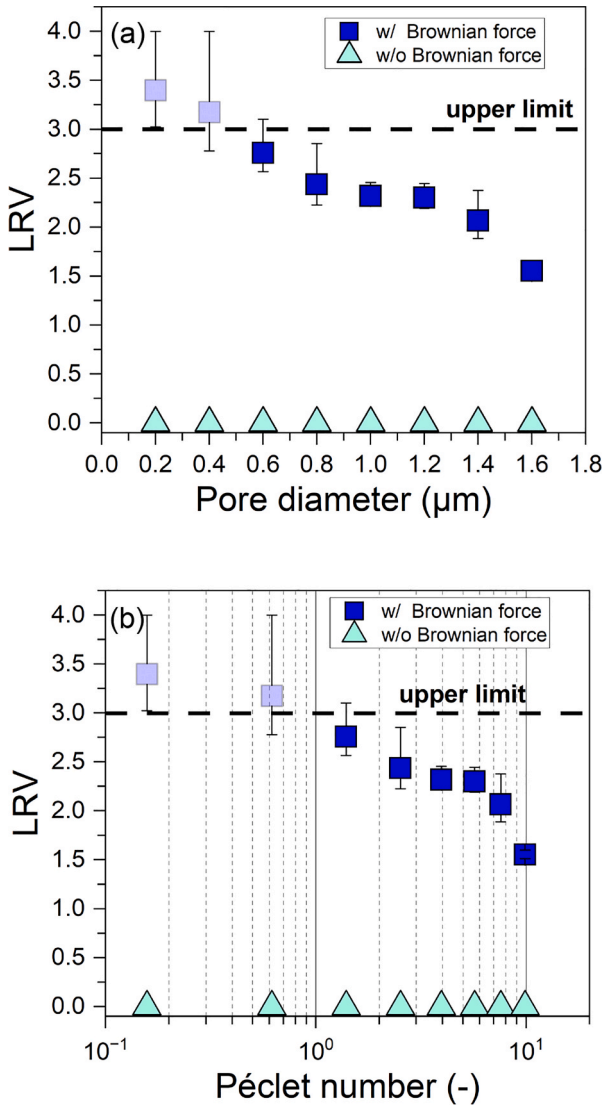

Fig. 1. Log reduction value (LRV) with and without Brownian force implemented in the flow model (a) for different pore diameters and (b) for corresponding Péclet numbers. The geometry consisted of straight pores with a length of 175 μm and pore diameters of 0.2, 0.4, 0.6, 0.8, 1.0, 1.2, 1.4, or 1.6 μm. Attachment coefficient = 10^{-1}. Triplicate simulations (n = 3) for each pore size were run: each data point represents the average LRV and one standard deviation. At the beginning of the simulation, 1000 particles were released at the inlet. Data above the upper limit (light-shade square) include at least one run with zero particles reaching the outlet, *i.e.*, all particles deposited on the pore walls.

The pore sizes of the simulation models in this study, *i.e.*, 0.2–1.6 μm, were larger than the nominal pore sizes of MF and UF membranes, *e.g.*, 0.1 μm and 0.01 μm, respectively. The nominal pore size is usually defined as the diameter of particles characterized by a 90 % removal rate; this implies that pore sizes are distributed, and a membrane includes pores characterized by a relatively large diameter range (Zeman and Zydney, 1996). The pore-size range employed in the simulation models represents the actual pore sizes characterizing a typical commercial MF membrane, as observed by scanning electron microscopy (Fig. S1). Although the results summarized in Fig. 1 were obtained for a specific pore structure and value of the attachment coefficient and may not necessarily extend to all geometries, they imply that there exist relevant conditions for which the LRV associated with internal deposition and driven by the Brownian force is not negligible. Therefore, the following sections investigate the relative effects of the pore structure and geometry on the mechanism of nanoparticle retention.

3.2. Influence of the attachment coefficient

The results presented in Fig. 2 (semi-log) indicate that the LRV associated with internal deposition increased monotonically with the attachment coefficient. In this simulation, Péclet number (Pe) was 1.4, suggesting that diffusive transport played a non-negligible role compared to convective transport driven by drag force. The trend was almost linear at a low attachment coefficient (< 10^{-2}) and became sublinear as the LRV approached the upper limit and very few particles reached the outlet. These results indicate that employing an appropriate attachment coefficient is important for estimating LRVs in actual membrane pores. However, it is to be noted that even at an attachment coefficient of 10^{-3}, which represents a relatively unfavorable attachment condition, a substantial fraction of particles was retained in the

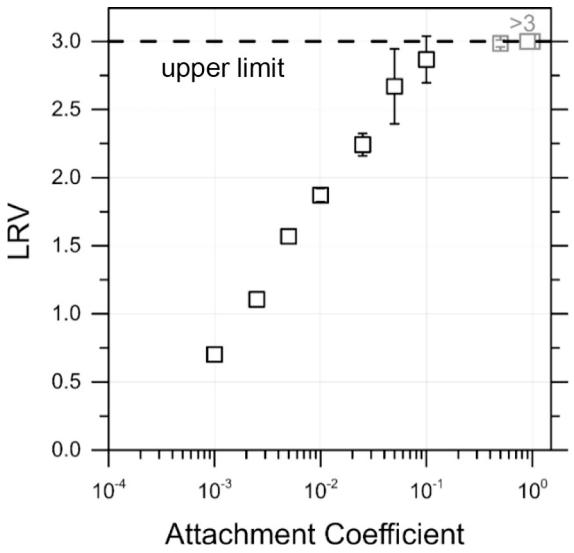

Fig. 2. Log reduction values (LRVs) for different attachment coefficients (n = 3). Simulation conditions: pore length = 175 μm; pore diameter = 0.6 μm; particle diameter = 0.02 μm; Pe = 1.4. Error bars represent one standard deviation. The maximum nominal LRV was 3 (dashed line), as 1000 particles were released at the inlet at the beginning of the simulation. Data at the upper limit (light-shade square) includes at least one run with zero particles reaching the outlet, *i.e.*, all particles deposited on the pore walls.

pores under the investigated conditions because of the high frequency of particle–wall collisions owing to Brownian force. Even at low values of the attachment coefficient, LRVs obtained from simulation models including Brownian force were greater than those (LRVs: 0.11–0.13) observed without Brownian force; see Fig. 1. Note that all the results presented in this manuscript and obtained at a fixed value of the attachment coefficient may be scaled to estimate the LRV with different prevailing attachment coefficients using the trend summarized in Fig. 2.

3.3. Effect of pore length

The results presented in Fig. 3 show that LRVs increased with pore length. In these simulations, the Péclet number (Pe) was 0.6 for a pore diameter of 0.4 μm and 2.5 for 0.8 μm, indicating that the influence of diffusion relative to the drag force was not negligible. Even implementing geometries with short pore lengths of 17.5 or 35 μm, LRVs were larger than 1.5 under the investigated conditions; this result suggests that the retention of particles occurred largely in the vicinity of the pore entrance, which was corroborated by a snapshot of the geometries following the simulations (*data not shown*). Interestingly, particle deposition to the pore walls close to the inlet was more prominent for the small pores (0.4 μm) than the large pores (0.8 μm). The simulation results suggest that when the pore length was extended, the LRV reached a plateau, which implies that for a given pore diameter, there might be an optimum pore length that would allow the maximization of the LRV and minimization of the membrane thickness. Moreover, with the larger pore diameter (0.8 μm), the pore length had a greater influence on LRV than with the smaller pore diameter (0.4 μm), for which a relatively high LRV was achieved even with a short length (Griffiths et al., 2020). The simulation results discussed in this work do not claim to represent absolute values of the LRV observed in real-world applications, but may be instead utilized to provide practical insights. In particular, in the case of Fig. 3, the data suggests that an optimum combination of pore diameter and membrane thickness may exist to achieve the target LRV with the highest flux for a given membrane material, when Brownian forces are not negligible.

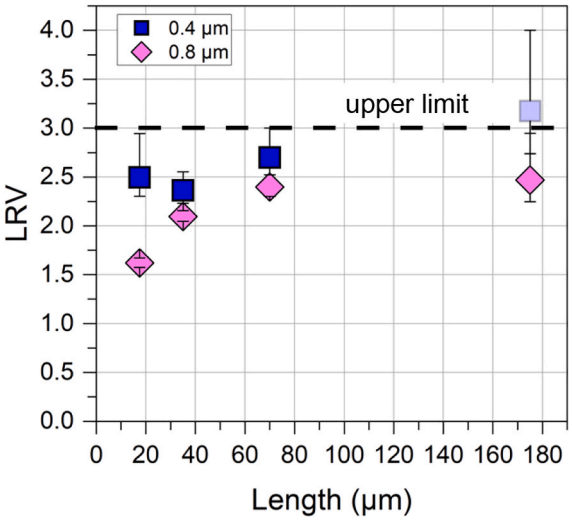

Fig. 3. Log reduction values (LRVs) for different lengths of straight pores (n = 3). Simulation conditions: straight pore; pore diameters = 0.4 or 0.8 μm; particle diameter = 0.02 μm; attachment coefficient = 10^{-1}; pore lengths: 17.5, 35, 70, or 175 μm; Pe = 0.6 (0.4 μm) or 2.5 (0.6 μm). Error bars represent one standard deviation. The maximum nominal LRV was 3 (dashed line), as 1000 particles were released at the inlet at the beginning of the simulation. The maximum computable LRV was 3 (dashed line) as 1000 particles were released at the inlet.

3.4. Effect of pore constriction

The results plotted in Fig. 4a show the effects of pore constrictions simulated as gates on the LRV. The attachment coefficient in these simulations was set at 5×10^{-3}. The LRV increased, and the flow velocity decreased with an increasing number of gates. The presence of gates influenced the LRVs in two ways: 1) it decreased the average flow velocity (as well as the Péclet number) and increased the HRT, and 2) it increased the probability of particle retention in the pore sections separated by the gates, where trajectories bent to pass through the narrow openings. It is interesting to note that installing a large number of gates in the large pore (pore diameter = 0.6 μm, gate number = 8 or 16) achieved both higher LRVs and higher fluxes than a geometry involving a small number of gates installed in a small pore (pore diameter = 0.3 μm, gate number = 2).

When analyzing the calculated LRV as a function of the Péclet number, the values of the former were linearly correlated with Pe for each of the pore diameters. Still, the slopes of the regression lines were different. The Péclet numbers varied in a small range for the 0.3-μm pores, approximately between 0.15 and 0.35, compared to the larger pores (0.6 μm, Pe range 0.4–1.2) (Fig. 4b). Additionally, the same LRVs were observed for different Pe numbers with the two pore sizes, for

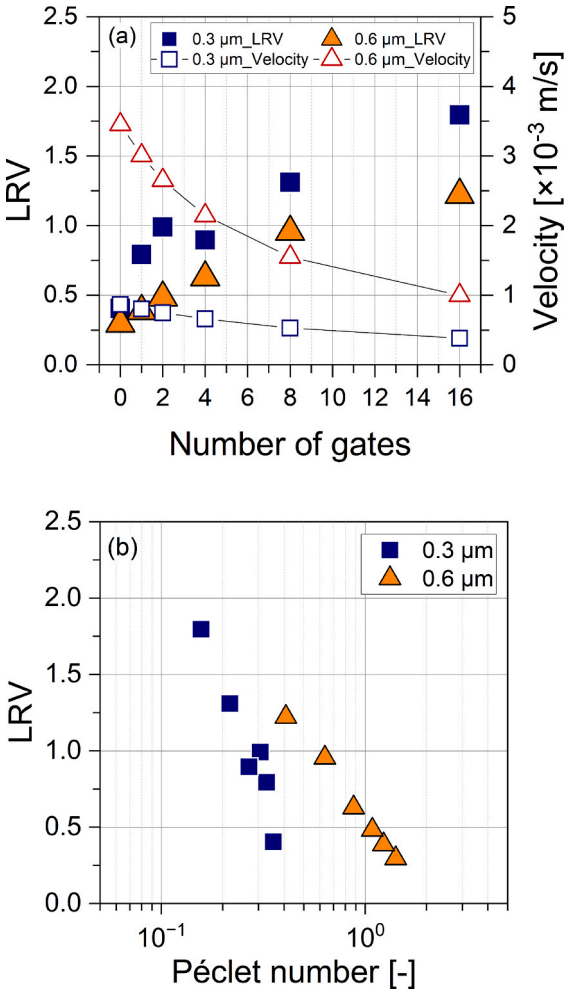

Fig. 4. Log reduction values (LRVs, closed symbols, left-hand axis) and average flow velocities (open symbols, right-hand axis) (a) for different numbers of gates and (b) for corresponding Péclet numbers (LRV only). Pore geometry: straight pores; pore length = 25 μm; pore diameter = 0.3 or 0.6 μm; particle diameter = 0.02 μm; attachment coefficient = 5×10^{-3}. Number of gates: 0, 1, 2, 4, 8, or 16. Average flow velocities were obtained by mediating across pore cross-sections.

example, LRV was approximately 0.45 at Pe ~ 0.35 and Pe ~ 1.1 for the smaller and larger pores, respectively. In contrast, at a similar Péclet number equal to approximately 0.35–0.4, LRV ~ 0.4 and LRV ~ 1.2 for the smaller and larger pores, respectively. These results may imply the following: although the Péclet number is an important parameter in delineating particle transport and attachment to membrane pore surfaces under the influence of both drag and Brownian forces, other factors such as pore diameter, surface area, and pore structure may also influence particle retention in the pores. In the geometry involving gates, the surface area was changed by approximately 13 % between the pores in the presence and absence of the gates (*data not shown*). Therefore, the constricted structure created by the gates had a dominant influence on the LRVs. The gates hindered particle transport between the pore segments separated by the gates and increased the retention time of the particles in each section. As a result, larger pore (0.6 μm), which incorporated gates, exhibited a higher LRV compared to smaller pore (0.3 μm), which had no or fewer gates.

Another interesting result relates to the porosity. Because the porosity of a membrane influences the water permeability and selectivity (Mehta and Zydney, 2005), porosity is considered one of the determining factors for the particle removal rates of porous membranes (Molnar et al., 2015). However, although pores with different numbers of gates had practically the same porosity, the related LRV varied significantly (Fig. 4a). These results suggest that pore structure, especially pore constriction, is a more important factor than overall porosity in influencing particle retention within the internal part of the membrane.

3.5. Effect of non-uniform pore diameter

The effects of pore constriction and morphology were also investigated using pore geometries involving non-uniform pore diameters (Table 1, Pore geometry 3). The pore models consisted of pores with two different diameters, *i.e.*, d_a and d_b: while d_a was fixed at either 0.3 μm or 0.6 μm, d_b was varied between 0.15 and 4 μm. The attachment coefficient was set at 5×10^{-3} for these simulations. In these simulations, Pe for $d_a = 0.3$ μm ranged from roughly 0.3 to 0.5 in the fixed region and from less than 0.1 to 0.3 in the variable region. For $d_a = 0.6$ μm, Pe ranged from approximately 1.4 to 2.7 in the fixed region and 0.5 to 1.4 in the variable region. Under both fixed region diameter conditions, the influence of diffusion relative to the drag force was not negligible. When d_a was 0.3 μm (Fig. 5a), LRV decreased from $d_b = 0.3$ μm, *i.e.*, a straight and uniform pore, to $d_b = 0.5$ μm, but then increased when d_b increased beyond this value. With $d_a = 0.6$ μm (Fig. 5a), the LRVs decreased when the alternate pore diameter increased from 0.15 μm to 0.6 μm (the latter referring to a straight and uniform pore), but then increased with the increasing value of d_b. That is, the same trend was observed for the two fixed pore sizes, d_a.

Although it is reasonable to assume that LRV would increase moving from a uniform pore to a non-uniform pore when $d_b < d_a$, namely, when portions of smaller size were introduced (similar to the introduction of gates), unexpectedly, LRV also increased when $d_b > d_a$, despite the greater porosity of this configuration compared to that characterizing a uniform pore of diameter d_a. Note that the LRV calculated in non-uniform configuration with very large d_b values (1.6 μm or larger) were substantially greater than those associated with uniform pores of diameter d_a, and certainly more than those associated with uniform pores of diameter d_b. Horizontal lines in Fig. 5a represent the LRV calculated for uniform pores with sizes of 0.3, 0.6, and 1.2 μm under the same conditions. This enhanced particle removal could be due to the increased particle retention in each pore segment provided by the complex morphology, including the constricted structures, regardless of the absolute values of the diameters of the pore portions (Chang et al., 2013). Note that LRV with $d_a = 0.3$ μm initially decreased when d_b exceeded d_a, as the accelerated flow velocity amplified the influence of drag force more significantly than in uniform pores. However, LRV increased again once d_b surpassed 0.6 μm, since further flow velocity growth became marginal. These results indicate that non-uniform pores with large variations in pore diameter (enlarging and/or reducing) may provide higher flux and greater LRVs than uniform pores with small diameters.

Because the configuration including non-uniform pores was characterized by a larger overall surface area compared with uniform pores, it is important to consider this effect on the LRV. Fig. 5b shows the LRVs presented in Fig. 5a, normalized by the inner surface areas of the respective pores. As d_b increased, the pore surface area also increased. The normalized LRV decreased monotonically as a function of d_b, implying that the surface area plays an important role. However, the LRVs were always higher for non-uniform pores than for uniform pores with diameter d_b (Fig. 5a), corroborating the role played by the constrictions rather than the more trivial effect ascribed to the surface area.

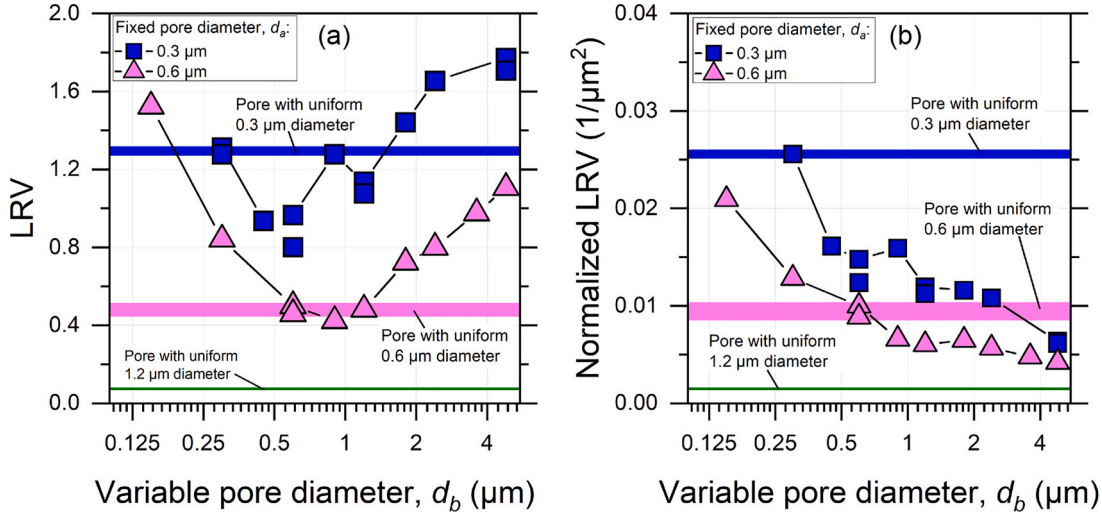

Fig. 5. Log removal values (LRVs) calculated with non-uniform pore diameters. (a) LRVs against d_b. (b) Normalized LRVs by the total inner surface area of pores against d_b. The horizontal bands are the ranges of LRVs or normalized LRVs for straight pores with uniform diameters of 0.3 μm (blue), 0.6 μm (pink), or 1.2 μm (green) (n = 3). Simulation conditions: pore length = 25 μm; attachment coefficient = 5×10^{-3}; the number of repetitions in the model geometry = 25; l_b/l_a length ratio = 1.

3.6. Effect of tortuosity

The results presented in Fig. 6 indicate that with an increase in the bending angle of the pore structure, LRVs increased noticeably. Apart from the bending angles, all the other simulation conditions, including the average length of the flow path, surface area, and pressure difference between the inlet and outlet, were identical. In these simulations, Péclet numbers were less than 0.4, indicating that the influence of diffusion relative to the drag force was not negligible. Note that at bending of 90°, the LRV decreased to the same level as 45°, which was probably due to the error associated with the fewer initial number of particles (1000 particles) in this simulation. In fact, LRVs haven't decreased and gotten its plateau in simulations with initial particle numbers of 5000 and 10,000 (data not shown). These results suggest that altering the flow direction by pore bending influences particle transport and deposition onto the pore walls (Griffiths et al., 2020; Sorci et al., 2020), implying that tortuosity may increase particle retention within the membrane pores.

3.7. Effect of pore size distribution

In geometries involving a parallel sequence that included one large pore and several small 0.3 μm pores available for particle entrance, LRVs were always in between those calculated for a single pore of small 0.3 μm diameter (or for a sequence of parallel pores, all of the same 0.3 μm diameter) and those calculated for a single pore of large diameter (or for a sequence of parallel pores all of the same large diameter), namely, 1.2 μm in Fig. 7a. More importantly, the LRV increased considerably with the number of small pores in the sequence (Fig. 7a), which indicates that the number of particles entering the small pores increased with the number of small pores. Note that the position of the large pores in the sequence, *e.g.*, at the end or the middle of the sequence, did not affect the results in terms of the LRV. Although the observed enhancement in the LRV seems to be easily explained by the conventional water flow model in pores, the calculated increment in the LRV was higher than that estimated based on the nominal rate of fluid flow into the pores and the particle retention rates associated with individual pores. These results are rationalized by the larger number of particles entering the small pores than those estimated by the laminar flow model, owing to the Brownian force that moves particles away from the main flow trajectory at the feed-membrane interface (Kim and Zydney, 2004), as corroborated by the data presented in Fig. S6 in the Supporting Information.

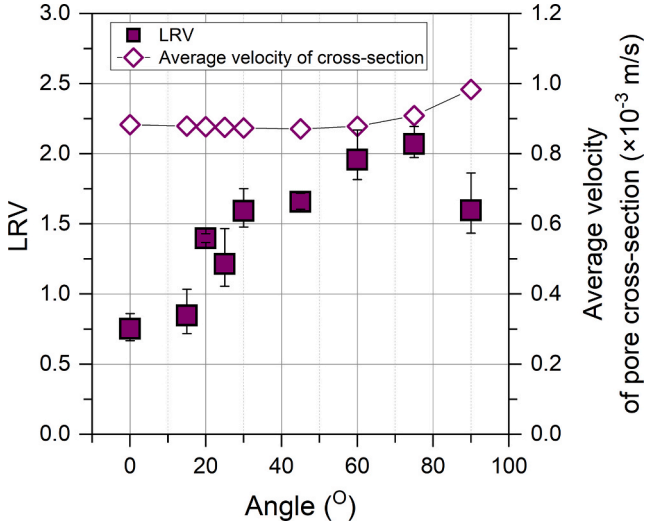

Fig. 6. Log reduction rate (LRV, closed square, left-hand axis) and average flow velocities (open diamond, right-hand axis) for different bending angles characterizing the pore geometry. Center pore length (length of the flow path) = 25 μm; pore diameter = 0.3 μm; attachment coefficient = 10^{-2}. Bending angles: 0°, 15°, 20°, 25°, 30°, 45°, 60°, 75°, 90° (n = 3 for each). Average flow velocities were obtained by mediating across pore cross-sections.

Similar results were obtained when the diameter of the large pore was changed in geometries comprising four small (0.3 μm) pores in parallel with one large pore. Specifically, calculated LRV were above those associated with pores characterized by the large diameter but smaller than those associated with the 0.3 μm pores. In addition, LRV decreased with the diameter of the large pores (Fig. 7b) because of the higher portion of fluid flow entering the increasingly large pores, wherein the particle retention rate was lower. These results again suggest that in the presence of small pores, LRVs were substantially higher than those predicted by laminar flow models (which underestimated the LRV; see Fig. S6). However, from a different standpoint, the presence of only one large pore among the many small pores considerably reduced the LRV with respect to the retention associated with a perfect sequence of small pores; this result implies that individual defects, *i.e.*, individual large pores, may result in a drop in the LRV provided by a membrane characterized by nominally small pore sizes. In other words, a defect-free membrane with medium-sized pores may be more advantageous regarding particle retention than a membrane with small pores and that comprises individual defects.

4. Discussion

The results presented in this study suggest that the Brownian force has a potential influence on nanoparticle transport in membrane pores under a practical range of conditions and is likely to increase the LRVs of nanoparticles by increasing the frequency of their collision with internal pore surfaces. Although the effect of the Brownian force was assumed to be negligible in previous studies (Mino et al., 2018; Mondal et al., 2019) that focused on particle separation in processes with Péclet numbers higher than 10^1 (Nelson and Ginn, 2011), this work implies that transport via the Brownian force may become more important than transport driven by the drag force at Péclet numbers smaller than 10^1, which is relevant for nanoparticle transport through MF or UF membranes in several instances (Liu et al., 2020; Yamamoto et al., 2014). Indeed, under strongly unfavorable attachment conditions, diffusive mechanisms would not result in a larger particle retention, since an enhanced collision rate due to Brownian forces would not translate into a significantly larger deposition rate. However, designing a membrane or a separation system to exploit Brownian forces may provide advantages in all other cases. In fact, the simulation results in this study agree with previous experimental study (Lee et al., 2020), which proposed diffusive deposition mechanism for the retention of inorganic nanoparticles in membrane filtration under conditions of low particle-to-pore diameter ratios (PPDs).

Viruses are nanoparticles of concern because virus infections can be caused by ingesting a small number of viruses (Kirby et al., 2014). In this sense, an enhancement of the total LRV by a value as low as 1, for example, from 5 to 6, owing to additional retention mechanisms occurring inside the membrane, may prove vital. Although understanding the behavior and retention of viruses in membrane pores is important for controlling the infection risks of drinking water, previous studies on virus transport within membrane pores are limited owing to the constraints of research tools (Bowen and Welfoot, 2002; Iliev et al., 2015). Virus removal rates measured in full-scale or pilot membrane filtration plants vary extensively, complicating the accurate evaluation of virus removal by membranes (Yasui et al., 2023). The simulation method presented in this study enabled the integration of drag and Brownian forces in diverse geometries to examine some of the basic mechanisms of nanoparticle transport, including viruses and retention in membrane pores. This approach is characterized by flexibility, which cannot be readily achieved in experimental studies.

Taking advantage of such simulations, this study suggests that complex pore structures, such as pore constriction and tortuosity, may

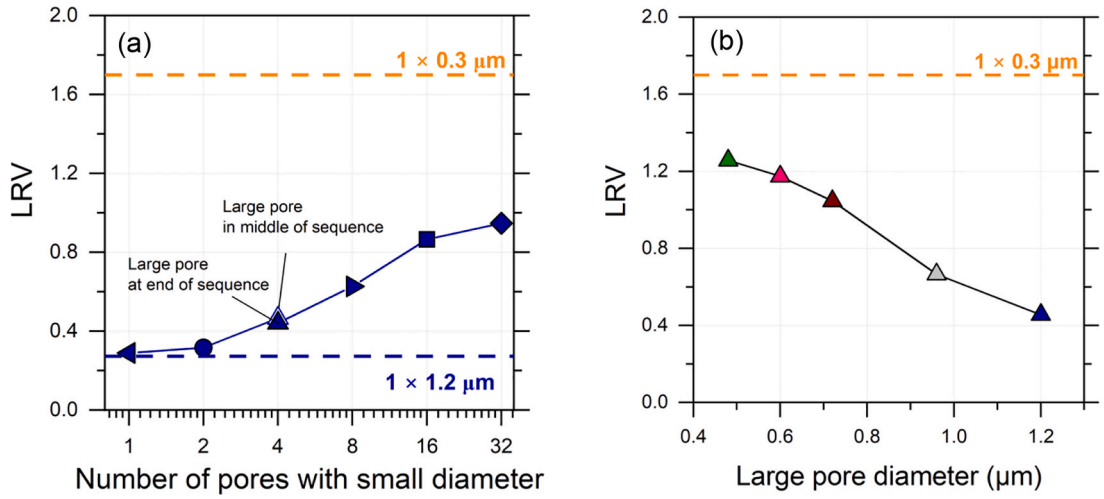

Fig. 7. Log reduction values (LRVs) of (a) geometries consisting of a variable number of small pores (0.3 μm) and one large pore (1.2 μm) and (b) geometries consisting of four 0.3 μm pores and one large pore with varying diameter, namely, 0.48 μm (green), 0.6 μm (red), 0.72 μm (brown), 0.96 μm (grey), and 1.2 μm (blue). The horizontal dash lines are the average LRVs computed by triplicate simulations with geometry consisting of a single straight pore (or a sequence of equal, straight pores) with diameters of 0.3 μm (orange) or 1.2 μm (blue). The simulations were conducted as follows: pore length = 25 μm; particles released in random positions at time = 0 within a 0.5 μm long anti-chamber preceding the sequence of pores; attachment coefficient = 10^{-2}.

affect nanoparticle transport and retention rates in membrane pores at Péclet numbers below 10^{1}, where the Brownian force becomes important. These structural factors have not been considered in association with the Brownian force in conventional cylindrical pore models that employ the hindered transport theory (Deen, 1987; ElHadidy et al., 2013). Specifically, the pore constriction, modeled as gates, increased the LRVs in correlation with the number of gates (Fig. 4a). Notably, although the LRV for the larger pore was generally lower than that for the smaller pore under uniform pore structure (Fig. 1a), the introduction of constricted structures in larger pore resulted in higher LRVs compared to smaller pores with straight geometries or fewer gates (Fig. 4b). Similarly, the LRVs for pores characterized by non-uniform diameters, comprising enlargements and constrictions, generally increased compared to straight pores of uniform diameter (Fig. 5). This phenomenon is attributed to a combination of factors, including the larger surface area of non-uniform pores, bent particle trajectories, and the complexity of the fluid velocity behavior within the pores (Fig. S3). As indicated in the previous simulation study (Su et al., 2019), the flow velocity in the wider segments of the pore was smaller than that in the narrower segments, which locally reduced the Péclet number and the probability of particles moving from the large to the small segments, resulting in an overall increase in LRVs (Fig. 5). However, although the tortuosity of the membrane pores did not affect the average flow velocity in a pore section, LRVs increased with higher tortuosity owing to the increase in the frequency of particle collisions onto the pore surface.

This study has certain limitations. First, future experimental studies shall reinforce the results of this study. Although controlling the Brownian force in the experiments is challenging, controlling the drag force by changing the filtration flux is possible. Thus, one might evaluate the comparative influence of the Brownian and drag forces on particle transport in membrane pores. Second, although 2D simulations of simple pore structures were employed to avoid simulation errors in complex 3D simulations and save CPU time, examining the differences and similarities between 2D and 3D membrane pore models is important because 3D models represent actual membrane pores. Although constructing 3D membrane pore models is challenging (Sundaramoorthi et al., 2016; Tan et al., 2023), studies deploying 3D models should verify the effects of Brownian forces on particle transport and removal within membrane pores.

Furthermore, it must be noted that, in this study, particles were treated as point masses without volume. This approach can be justified because the particles were highly diluted in the simulations, with typical concentrations lower than 10^{13} particles per mL. Because of this assumption of dilute solution, our simulation applies to the initial stage of filtration. Therefore, further simulation of particle deposition within pores occurring at later stages of the filtration process would help delineate any pore blocking processes. Finally, we varied the attachment coefficient between 10^{-3} and 10^{-1} to highlight the effects of pore structures on retention, consistent with previously estimated values where 10^{-3} represents mildly unfavorable conditions and 10^{-1} represents near favorable conditions for nanoparticle attachment to porous media surfaces (Hahn and O'Melia, 2004; Tufenkji and Elimelech, 2005b). Those studies suggested that the interaction energy profile between nanoparticles and surfaces governs the attachment and detachment of nanoparticles from surfaces (Hahn and O'Melia, 2004; Tufenkji and Elimelech, 2005b). Moreover, recent studies have advanced theoretical frameworks regarding the extended DLVO theory and factors influencing attachment coefficients, including solution ionic strength, hydrodynamic shear, Brownian diffusion, and particle sizes (Lee et al., 2019; Wang et al., 2016). It is noteworthy that when the interaction energy between the particle and the membrane surface is relatively weak—such as when the particle is retained within the secondary energy minimum—hydrodynamic forces may induce particle detachment and subsequent release from the membrane surface (Lee et al., 2017). Therefore, in future studies, it is recommended to use actual attachment coefficients obtained from theoretical and experimental studies to estimate truthful LRVs. Additionally, experimental validation using virus particles with varying sizes and surface characteristics, combined with filtration membranes possessing different nominal pore sizes, membrane structures, and materials, will help elucidate the influence of Brownian forces on viral particle retention and clarify the underlying retention mechanisms.

Finally, note that this study does not provide factual, absolute LRVs related to particle or virus deposition within real membrane pores. However, this study revealed relative effects of Brownian force and pore structures on particle retention that may have been overlooked previously. Also, simulation results highlighted the factors influencing retention performance owing to the Brownian force under various operational conditions. These factors include the relationship between the attachment coefficient and LRV (Fig. 2), the effect of pore length on LRV (Fig. 3), and the linear relationship between the Péclet number and LRV (Fig. 4b). These results may be used to estimate LRVs in given

membrane pore structures and/or to design membrane pore structures with high LRVs without sacrificing membrane permeance and productivity. In particular, according to the results presented in this paper, a better porous membrane may be designed with the following characteristics to simultaneously augment flux and nanoparticle LRV; namely, the keys for designing high flux and particle retention membranes are: (i) high tortuosity, (ii) non-uniform internal pore diameters with the presence of constrictions and enlargements, and (iii) uniform surface pore size with the absence of defects.

5. Conclusions

The results shown in this study indicate that the Brownian force may be important for particle transport in membrane pores with Péclet numbers smaller than 10^1. Although the previous studies assumed that the overall porosity is a determinant factor of particle retention inside membrane pores, this study does not corroborate this assumption, indicating that the complexity of pore structures is more consequential for internal particle retention. The constriction and tortuosity of the membrane pores and the non-uniform pore structure significantly affected the LRVs of the nanoparticles under the influence of the Brownian force in the simulated 2D geometries. In a parallel pore structure with large and small pore diameters, the Brownian force increases the number of particles entering the membrane through small pores in relation to the number estimated based on the laminar flow rates. This indicates the importance of small pores and, in contrast, the detrimental impact of individual defects in filtration membranes. The relationship between the attachment coefficient and LRV, and the effect of pore structure on LRV, may be useful for designing membrane pore structures with high LRVs without sacrificing membrane permeance.

Although this study is based solely on simulations and provides relative effects rather than absolute LRVs, experimental studies in the future will further reinforce the simulation results presented herein. In addition, the 2D pore models used in this study should be extended to 3D models representing actual pore structures. Nevertheless, our study identified the Brownian force as an important mechanism of transport and retention of nanoparticles within membrane pores, which may provide a non-negligible LRV of nanoparticles in pores under diverse conditions. The methods presented in this paper can be applied to membrane pores in future studies.

CRediT authorship contribution statement

Takashi Hashimoto: Writing – original draft, Visualization, Software, Methodology, Investigation, Funding acquisition, Formal analysis. **Alberto Tiraferri:** Writing – review & editing, Visualization, Software, Methodology, Investigation, Formal analysis. **Satoshi Takizawa:** Writing – review & editing, Validation, Software, Resources, Investigation, Funding acquisition, Conceptualization.

Funding

This study was supported by a Grant-in-Aid for Scientific Research (No. 22H01621) from the Japan Society for the Promotion of Sciences (JSPS) and “Advanced Research Infrastructure for Materials and Nanotechnology in Japan (ARIM)” of the Ministry of Education, Culture, Sports, Science and Technology (MEXT), Grant Number JPMXP1223UT0120.

Declaration of competing interest

The authors declare that they have no known competing financial interests or personal relationships that could have appeared to influence the work reported in this paper.

Acknowledgments

The authors wish to thank Tokyo College for providing opportunities for research collaboration.

Appendix A. Supplementary data

Supplementary data to this article can be found online at https://doi.org/10.1016/j.ces.2025.122010.

Data availability

Data will be made available on request.

References

Boccardo, G., Sethi, R., Marchisio, D.L., 2019. Fine and ultrafine particle deposition in packed-bed catalytic reactors. Chem. Eng. Sci. 198, 290–304. https://doi.org/10.1016/j.ces.2018.09.024.

Bowen, W.R., Welfoot, J.S., 2002. Modelling of membrane nanofiltration—pore size distribution effects. Chem. Eng. Sci. 57, 1393–1407. https://doi.org/10.1016/S0009-2509(01)00412-2.

Brant, J.A., Childress, A.E., 2002. Membrane–colloid interactions: Comparison of extended DLVO predictions with AFM force measurements. Environ. Eng. Sci. 19, 413–427. https://doi.org/10.1089/109287502320963409.

Brenner, H., Gaydos, L.J., 1977. The constrained brownian movement of spherical particles in cylindrical pores of comparable radius. J. Colloid Interface Sci. 58, 312–356. https://doi.org/10.1016/0021-9797(77)90147-3.

Calo, V.M., Iliev, O., Lakdawala, Z., Leonard, K.H.L., Printsypar, G., 2015. Pore-scale modeling and simulation of flow, transport, and adsorptive or osmotic effects in membranes: the influence of membrane microstructure. Int. J. Adv. Eng. Sci. Appl. Math. 7, 2–13. https://doi.org/10.1007/s12572-015-0132-3.

Chang, Y.I., Liao, K.Y., Jiang, C.H., 2013. Motion of particle breakthrough curve and permeability reduction in voronoi and triangular networks. Sep. Purif. Technol. 114, 38–42. https://doi.org/10.1016/j.seppur.2013.04.006.

Chaudhry, R.M., Holloway, R.W., Cath, T.Y., Nelson, K.L., 2015. Impact of virus surface characteristics on removal mechanisms within membrane bioreactors. Water Res. 84, 144–152. https://doi.org/10.1016/j.watres.2015.07.020.

Dalwadi, M.P., Griffiths, I.M., Bruna, M., 2015. Understanding how porosity gradients can make a better filter using homogenization theory. Proc. r. Soc. A Math. Phys. Eng. Sci. 471, 20150464. https://doi.org/10.1098/rspa.2015.0464.

Dechadilok, P., Deen, W.M., 2006. Hindrance factors for diffusion and convection in pores. Ind. Eng. Chem. Res. 45, 6953–6959. https://doi.org/10.1021/ie051387n.

Deen, W.M., 1987. Hindered transport of large molecules in liquid-filled pores. AIChE J. 33, 1409–1425. https://doi.org/10.1002/aic.690330902.

ElHadidy, A.M., Peldszus, S., Van Dyke, M.I., 2013. An evaluation of virus removal mechanisms by ultrafiltration membranes using MS2 and φX174 bacteriophage. Sep. Purif. Technol. 120, 215–223. https://doi.org/10.1016/j.seppur.2013.09.026.

Gerba, C.P., Betancourt, W.Q., Kitajima, M., 2017. How much reduction of virus is needed for recycled water: a continuous changing need for assessment? Water Res. 108, 25–31. https://doi.org/10.1016/j.watres.2016.11.020.

Ghanbarian, B., Hunt, A.G., Ewing, R.P., Sahimi, M., 2013. Tortuosity in porous media: a critical review. Soil Sci. Soc. Am. J. 77, 1461–1477. https://doi.org/10.2136/sssaj2012.0435.

Giglia, S., Bohonak, D., Greenhalgh, P., Leahy, A., 2015. Measurement of pore size distribution and prediction of membrane filter virus retention using liquid-liquid porometry. J. Memb. Sci. 476, 399–409. https://doi.org/10.1016/j.memsci.2014.11.053.

Graczyk, K.M., Matyka, M., 2020. Predicting porosity, permeability, and tortuosity of porous media from images by deep learning. Sci. Rep. 10, 21488. https://doi.org/10.1038/s41598-020-78415-x.

Griffiths, I.M., Mitevski, I., Vujkovac, I., Illingworth, M.R., Stewart, P.S., 2020. The role of tortuosity in filtration efficiency: a general network model for filtration. J. Memb. Sci. 598, 117664. https://doi.org/10.1016/j.memsci.2019.117664.

Gu, B., Renaud, D.L., Sanaei, P., Kondic, L., Cummings, L.J., 2020. On the influence of pore connectivity on performance of membrane filters. J. Fluid Mech. 902, A5. https://doi.org/10.1017/jfm.2020.520.

Gustafsson, O., Gustafsson, S., Manukyan, L., Mihranyan, A., 2018. Significance of brownian motion for nanoparticle and virus capture in nanocellulose-based filter paper. Membranes (basel). 8. https://doi.org/10.3390/membranes8040090.

Hahn, M.W., O’Melia, C.R., 2004. Deposition and reentrainment of brownian Particles in porous media under unfavorable chemical conditions: some concepts and applications. Environ. Sci. Technol. 38, 210–220. https://doi.org/10.1021/es030416n.

Hashimoto-Gotoh, A., Matuki, T., Miyazawa, T., 2015. Evaluation of membrane filtration system using the “pore diffusion” for eliminating viruses. J. Vet. Med. Sci. 77, 733–737. https://doi.org/10.1292/jvms.14-0625.

Huang, H., Young, T.A., Schwab, K.J., Jacangelo, J.G., 2012. Mechanisms of virus removal from secondary wastewater effluent by low pressure membrane filtration. J. Memb. Sci. 409–410, 1–8. https://doi.org/10.1016/j.memsci.2011.12.050.

Iliev, O., Lakdawala, Z., Leonard, K., Vutov, Y., 2015. On pore-scale modeling and simulation of reactive transport in 3D geometries.
Iliev, O., Lakdawala, Z., Neßler, K.H.L., Prill, T., Vutov, Y., Yang, Y., Yao, J., 2017. On the pore-scale modeling and simulation of reactive transport in 3D geometries. Math. Model. Anal. 22, 671–694. https://doi.org/10.3846/13926292.2017.1356759.
Israelachvili, J.N., 2011. Intermolecular and Surface forces. Third Edit. Ed. Elsevier. https://doi.org/10.1016/C2009-0-21560-1.
Kim, M.M., Zydney, A.L., 2004. Effect of electrostatic, hydrodynamic, and brownian forces on particle trajectories and sieving in normal flow filtration. J. Colloid Interface Sci. 269, 425–431. https://doi.org/10.1016/j.jcis.2003.08.004.
Kirby, A.E., Shi, J., Montes, J., Lichtenstein, M., Moe, C.L., 2014. Disease course and viral shedding in experimental Norwalk virus and Snow Mountain virus infection. J. Med. Virol. 86, 2055–2064. https://doi.org/10.1002/jmv.23905.
Lee, H., Segets, D., Süß, S., Peukert, W., Chen, S.-C.-C., Pui, D.Y.H., 2017a. Liquid filtration of nanoparticles through track-etched membrane filters under unfavorable and different ionic strength conditions: Experiments and modeling. J. Memb. Sci. 524, 682–690. https://doi.org/10.1016/j.memsci.2016.11.023.
Lee, H., Kim, S.C., Chen, S.C., Segets, D., Pui, D.Y.H., 2019. Predicting collision efficiencies of colloidal nanoparticles in single spherical and fibrous collectors using an individual particle tracking method. Sep. Purif. Technol. 222, 202–213. https://doi.org/10.1016/j.seppur.2019.04.025.
Lee, H., Segets, D., Süß, S., Peukert, W., Chen, S.-C., Pui, D.Y.H., 2020. Effects of filter structure, flow velocity, particle concentration and fouling on the retention efficiency of ultrafiltration for sub-20 nm gold nanoparticles. Sep. Purif. Technol. 241, 116689. https://doi.org/10.1016/j.seppur.2020.116689.
Lee, S., Ihara, M., Yamashita, N., Tanaka, H., 2017b. Improvement of virus removal by pilot-scale coagulation-ultrafiltration process for wastewater reclamation: effect of optimization of pH in secondary effluent. Water Res. 114, 23–30. https://doi.org/10.1016/j.watres.2017.02.017.
Ley, A., Altschuh, P., Thom, V., Selzer, M., Nestler, B., Vana, P., 2018. Characterization of a macro porous polymer membrane at micron-scale by confocal-laser-scanning microscopy and 3D image analysis. J. Memb. Sci. 564, 543–551. https://doi.org/10.1016/j.memsci.2018.07.062.
Liu, S.Y., Chen, Z., Sanaei, P., 2020. Effects of Particles diffusion on membrane filters performance. Fluids 5, 121. https://doi.org/10.3390/fluids5030121.
Matyka, M., Khalili, A., Koza, Z., 2008. Tortuosity-porosity relation in porous media flow. phys. rev. E - stat. Nonlinear, Soft Matter Phys. 78, 1–8. https://doi.org/10.1103/PhysRevE.78.026306.
Mehta, A., Zydney, A.L., 2005. Permeability and selectivity analysis for ultrafiltration membranes. J. Memb. Sci. 249, 245–249. https://doi.org/10.1016/j.memsci.2004.09.040.
Mino, Y., Sakai, S., Matsuyama, H., 2018. Simulations of particulate flow passing through membrane pore under dead-end and constant-pressure filtration condition. Chem. Eng. Sci. 190, 68–76. https://doi.org/10.1016/j.ces.2018.05.061.
Molnar, I.L., Johnson, W.P., Gerhard, J.I., Willson, C.S., O'Carroll, D.M., 2015. Predicting colloid transport through saturated porous media: a critical review. Water Resour. Res. 51, 6804–6845. https://doi.org/10.1002/2015WR017318.
Molnar, I.L., Sanematsu, P.C., Gerhard, J.I., Willson, C.S., O'Carroll, D.M., 2016. Quantified pore-scale nanoparticle transport in porous media and the implications for colloid filtration theory. Langmuir 32, 7841–7853. https://doi.org/10.1021/acs.langmuir.6b01233.
Mondal, S., Griffiths, I.M., Ramon, G.Z., 2019. Forefronts in structure–performance models of separation membranes. J. Memb. Sci. 588, 117166. https://doi.org/10.1016/j.memsci.2019.06.006.
Nelson, K.E., Ginn, T.R., 2011. New collector efficiency equation for colloid filtration in both natural and engineered flow conditions. Water Resour. Res. 47, 1–17. https://doi.org/10.1029/2010WR009587.
Sanaei, P., Cummings, L.J., 2017. Flow and fouling in membrane filters: effects of membrane morphology. J. Fluid Mech. 818, 744–771. https://doi.org/10.1017/jfm.2017.102.
Sano, D., Amarasiri, M., Hata, A., Watanabe, T., Katayama, H., 2016. Risk management of viral infectious diseases in wastewater reclamation and reuse: review. Environ. Int. 91, 220–229. https://doi.org/10.1016/j.envint.2016.03.001.
Sorci, M., Woodcock, C.C., Andersen, D.J., Behzad, A.R., Nunes, S., Plawsky, J., Belfort, G., 2020. Linking microstructure of membranes and performance. J. Memb. Sci. 594, 117419. https://doi.org/10.1016/j.memsci.2019.117419.
Su, J., Chai, G., Wang, L., Cao, W., Gu, Z., Chen, C., Xu, X.Y., 2019. Pore-scale direct numerical simulation of particle transport in porous media. Chem. Eng. Sci. 199, 613–627. https://doi.org/10.1016/j.ces.2019.01.033.
Sundaramoorthi, G., Hadwiger, M., Ben-Romdhane, M., Behzad, A.R., Madhavan, P., Nunes, S.P., 2016. 3D membrane imaging and porosity visualization. Ind. Eng. Chem. Res. 55, 3689–3695. https://doi.org/10.1021/acs.iecr.6b00387.
Tan, D.Y., Hashimoto, T., Takizawa, S., 2023. 3D modeling of PVDF membrane aging using scanning electron microscope and OpenCV image analysis. J. Memb. Sci. 666, 121141. https://doi.org/10.1016/j.memsci.2022.121141.
Trzaskus, K.W., de Vos, W.M., Kemperman, A., Nijmeijer, K., 2015. Towards controlled fouling and rejection in dead-end microfiltration of nanoparticles - role of electrostatic interactions. J. Memb. Sci. 496, 174–184. https://doi.org/10.1016/j.memsci.2015.06.047.
Tufenkji, N., Elimelech, M., 2005a. Spatial distributions of cryptosporidium oocysts in porous media: evidence for dual mode deposition. Environ. Sci. Technol. 39, 3620–3629. https://doi.org/10.1021/es048289y.
Tufenkji, N., Elimelech, M., 2005b. Breakdown of colloid filtration theory: role of the Secondary energy minimum and Surface Charge heterogeneities. Langmuir 21, 841–852. https://doi.org/10.1021/la048102g.
Tufenkji, N., Elimelech, M., 2004. Deviation from the classical colloid filtration theory in the presence of repulsive DLVO interactions. Langmuir 20, 10818–10828. https://doi.org/10.1021/la0486638.
Wang, Z., Jin, Y., Shen, C., Li, T., Huang, Y., Li, B., 2016. Spontaneous detachment of colloids from Primary energy minima by brownian diffusion. PLoS One 11, e0147368. https://doi.org/10.1371/journal.pone.0147368.
Yamamoto, A., Hongo-Hirasaki, T., Uchi, Y., Hayashida, H., Nagoya, F., 2014. Effect of hydrodynamic forces on virus removal capability of Planova^{TM} filters. AIChE J. 60, 2286–2297. https://doi.org/10.1002/aic.14392.
Yao, K.-M., Habibian, M.T., O'Melia, C.R., 1971. Water and waste water filtration. Concepts and Applications. Environ. Sci. Technol. 5, 1105–1112. https://doi.org/10.1021/es60058a005.
Yasui, M., Ikner, L., Yonetani, T., Liu, M., Katayama, H., 2023. Effects of surface hydrophobicity on the removal of F-specific RNA phages from reclaimed water by coagulation and ceramic membrane microfiltration. Water Sci. Technol. 87, 2304–2314. https://doi.org/10.2166/wst.2023.133.
Yasui, M., Wang, X., Tarabara, V.V., Katayama, H., 2024. Virus removal by microfiltration: effects of electrostatic and hydrophobic interactions. Sep. Purif. Technol. 350, 127902. https://doi.org/10.1016/j.seppur.2024.127902.
Yin, Z., Tarabara, V.V., Xagoraraki, I., 2015. Human adenovirus removal by hollow fiber membranes: effect of membrane fouling by suspended and dissolved matter. J. Memb. Sci. 482, 120–127. https://doi.org/10.1016/j.memsci.2015.02.028.
Zeman, L.J., Zydney, A.L., 1996. Microfiltration and ultrafiltration: principles and applications, 1st ed. Marcel Dekker Inc., New York.